Characterizing the spatiotemporal distribution of meteorological drought as a response to climate variability: The case of rift valley lakes basin of Ethiopia

Birhane Gebrehiwot Tesfamariam [a,b,*], Berhan Gessesse [b], Farid Melgani [c]

[a] Department of Land Administration and Surveying, Dilla University, P.O.Box 419, Ethiopia
[b] Department of Remote Sensing, Entoto Observatory and Research Center, Ethiopian Space Science and Technology Institute (ESSTI), Addis Ababa, Ethiopia
[c] Department of Information Engineering and Computer Science, University of Trento, Italy

A B S T R A C T

Climate variability and recurrent meteorological droughts frequently affect the rain-dependent Ethiopian agriculture, where the rift valley lakes basin is one of the most drought-prone regions in the country. The aim of this study was to evaluate climate variability and characterize the spatiotemporal distribution of meteorological droughts using a merged satellite-gauge rainfall across the major agroecological zones (AEZs) of the rift valley lakes basin. To this end, coefficient of variation (CV) and standardized rainfall anomaly (SRA) were used to evaluate rainfall variability; Mann-Kendell test was used to examine trends of temperature and rainfall; and a grid-rainfall based standardized precipitation index (SPI) was used to assess the spatiotemporal distribution and severity of meteorological droughts. The SPI was computed for 37 years over 1981–2017 at 3-month and 4-month timescales for the bimodal rainy seasons. Finally, a higher inter-annual and spatial variability of rainfall and frequent meteorological droughts were found across the basin. Compared to the nationally documented historical drought years in the country, more frequent drought events were found in this basin, signifying its higher vulnerability to climate variability. As a result, between 1981 and 2017, the basin has partially experienced at least a moderate drought intensity on average every 1.68 and 1.76 years during the 'Belg' and 'Kiremt' season, respectively. Drought frequency was higher at the 'Kolla' AEZ, characterized by the highest CV of rainfall. Furthermore, these frequent droughts were accompanied by significant rising trends in monthly temperature. Such a warming trend, in this inherently warm area, coupled with expected global climate change scenarios could further aggravate drought conditions in the future. Moreover, the spatiotemporal distribution of drought events was found to be variable between and within AEZs in the basin so that more localized drought adaptation strategies could help to alleviate potential impacts. Thus, the drought history of each agroecological zone and the spatiotemporal distributions of recent droughts, this study has delivered, could enhance the awareness of concerned decision makers in tracing frequently affected locations, which could in turn enable them to design and implement improved water management techniques as a means of drought mitigation strategy.

1. Introduction

Livelihood of the majority Ethiopian population predominantly depends on rain-fed agriculture (Agricultural Transformation Agency, 2014), which is however, highly vulnerable to extreme weather events primarily recurrent drought hazards (World-Bank, 2006). Due to the strong dependence of the population on rain-fed agricultural livelihoods, many of the drought hazards have caused devastating losses of human and livestock lives in different parts of the country (Mohammed et al., 2017; Degefu and Bewket, 2014). Such catastrophes usually significantly affect the national GDP of the country. For instance, during the 1984–1985 drought, one of the most devastating drought periods in the country, the national GDP was dropped by 9.7%, while agricultural output was further declined by 21%. Besides, long lasting drought incidences can also reduce the potentials of hydroelectric power generation, the leading power source of the country (World-Bank, 2006). Moreover, although drought is a naturally occurring climate anomaly (WMO, 2012; Wilhite, 1993), future climate change scenarios are likely

to further intensify its impacts particularly over the sub-Saharan Africa (Thornton et al., 1934; Boko et al., 2007).

On the other hand, the teleconnection between Ethiopian droughts and the fluctuation in global sea surface temperature is already known (Degefu et al., 2017; Fekadu, 2015; Funk et al, 2008, 2014a; Williams et al., 2012; Alory et al., 2007; Cai et al., 2007; Verdin et al., 2005; Barnett et al., 2001). However, since the country is characterized by a complex and wider topographic variations (from 130 m below sea level to 4620 m above sea level), there is a great hydroclimate variation in terms of amount, spatial distribution, and seasonality of rainfall (Viste et al., 2013; Dinku et al., 2008). As such, in addition to the effects of fluctuations in global sea surface temperatures (SSTs) which primarily cause droughts, the Ethiopian hydroclimate is inherently complex, confounded by the complexity of local topography resulting in varied microclimates and varying vulnerability to meteorological droughts. (Viste, 2012; Jury, 2010; Edossa et al., 2010; Dinku et al., 2007). For instance, across parts of the southern, southwestern, and southeastern Ethiopia, the Spring (locally 'Belg' season, March–May) and the Summer (locally 'Kiremt' season, June–September) rainfall has reportedly declined by 15–20 percent between the mid-1970s and late 2000s (USAID, 2012). Similarly, Viste, Korecha (Viste et al., 2013) has also reported a declining trend of annual rainfall amounts, particularly in southern Ethiopia (including part of the present study area) from 1971 to 2011 during both the 'Belg' and 'Kiremt' seasons. Throughout this period (1971–2011), the largest relative precipitation deficit was also observed in the southern parts of the country during the 'Belg', the main rainy season of southernmost Ethiopia (Viste et al., 2013). As a result, the rift valley region in general (including the present study area) is known to be one of the two hot-spot areas in the country more vulnerable to climate variability (Viste et al., 2013; USAID, 2012). By contrast, in spite of this reality, the rift valley lakes basin is heavily populated compared to all other basins in the country (USAID, 2012; MoWE, 2014; Funk et al., 2005), which encompasses areas having a population density of greater than 200 people per square kilometer. Thus, the recurrent drought incidences coupled with such a huge population number challenges ensuring food security in this basin.

In response to the recurrent nation-wide and local-scale meteorological drought incidences in Ethiopia, assessment studies were carried out in different parts of the country [for example, Asfaw et al., 2018, Gidey et al., 2018, Mohammed et al., 2017, Degefu and Bewket, 2014, Viste et al., 2013, Kassie et al., 2013, Gebrehiwot et al., 2011, Degefu and Glantz, 1987]. However, despite the fact that the rift valley lakes basin is on the top of drought-prone regions in the country, very little is known about the spatial and temporal characteristics of meteorological droughts in the basin. Moreover, analysis of climate variability and spatiotemporal distributions of drought events considering the different agroecological zones, is one of the crucial, but the missing research component, particularly in the study area. Therefore, in view of the inherent diverse microclimates characterizing the country, this study attempts to analyze climate variability and the spatiotemporal distributions of recent meteorological droughts across agroecological zones (AEZs) in the rift valley lakes basin to better characterize and understand local climatic variations.

Since rainfall is a variable climate element over space and time (Mishra, 2013), sufficient ground-measured rainfall data from evenly distributed rain gauge network is required in order to carry out reliable drought assessment studies. However, the density of the rain gauge stations in the study area, especially those with historical rainfall records, is very sparse and unevenly distributed. Hence, in order to prevent absolute dependence on these inadequate gauge observations, the available rain gauge stations were used to correct the bias of a satellite rainfall estimate so as to synthesize a merged satellite-gauge rainfall product. Accordingly, the Climate Hazards group Infrared Precipitation with Stations version 2.0 (hereafter CHIRPS) was merged with the ground-measured rainfall data using a proper bias-adjustment technique. Among a plentiful of satellite rainfall products, CHIRPS was

preferred for this purpose due its longtime historical rainfall record and higher spatial resolutions (for details, refer section 2.3). More importantly, its skill of retrieving observed rainfall was found to be comparatively better (Tesfamariam et al., 2019; Dinku et al., 2018; Ayehu et al., 2018; Trejo et al., 2016; Toté et al., 2015); and its suitability for monitoring meteorological drought events was also verified (Tesfamariam et al., 2019; Bayissa et al., 2017). As satellite-derived rainfall products play a leading role to overcome the inadequacy of rain gauge density (Dinku et al., 2013; Kidd and Huffman, 2011; Kidd and Levizzani, 2011), the merged satellite-gauge rainfall grid was finally used to calculate a pixel-based standardized precipitation index (SPI) to characterize the spatiotemporal distributions of meteorological droughts. This blended rainfall product is considered to be an ideal geospatial tool to understand the spatial extent and spatial distributions of drought events across agroecological zones in the basin. Because the socioeconomic and environmental impacts of a drought event is determined by its spatial distribution in addition to its magnitude, duration, and frequency (Zargar et al., 2011; Bannayan et al., 2010).

Therefore, this study attempts to investigate climate variability in terms of annual and seasonal rainfall fluctuations and monthly temperature trends, and more importantly focus on the analysis of spatiotemporal dynamics of seasonal meteorological droughts across agroecological zones in the rift valley lakes basin of Ethiopia. To realize this objective, a blended satellite-gauge rainfall grid covering about four decades (1981–2017) was used as a principal rainfall data to characterize rainfall variability and the spatiotemporal distribution of seasonal drought events against agroecological categories. Besides, ground-measured rainfall and temperature data were used for trend analysis and significance test. As a first of its kind in this basin, to the best of our knowledge, typically carried out by integrating gauge-measured and more accurate satellite rainfall estimates, the results of this study could greatly help concerned decision makers to understand the spatiotemporal dynamics of meteorological droughts to subsequently design appropriate drought mitigation and early warning systems for the basin.

2. Materials and methods

2.1. Description of the study area

The rift valley lakes basin is part of the Great African Rift in Southern Ethiopia, geographically located between 4.37° to 8.47° N and 36.59° to 39.41° E covering a total surface area of 53,054.05 square kilometers (MoWE, 2014). It is surrounded by the Awash Basin in the north, Omo-Ghibe Basin in the west, Genale-Dawa Basin in southeast, and by Wabi Sheble Basin in the east (Fig. 1). The basin is predominantly characterized by a moderate tropical semiarid climate having a bimodal rainfall distributions, with the short rainy season ('Belg') extending from
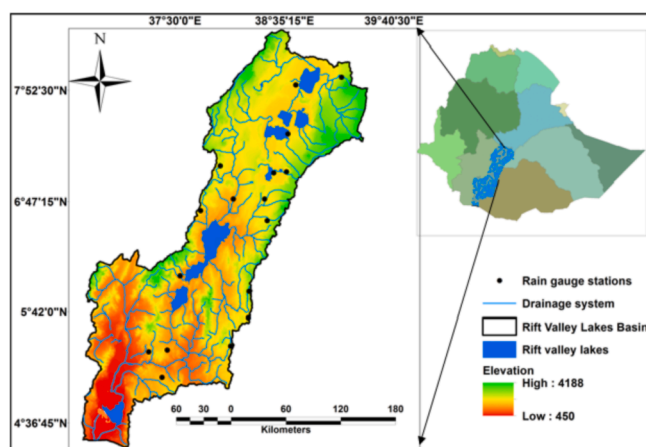

Fig. 1. Location map of the rift valley lakes basin.

March to May and the long rainy season ('*Kiremt*') from June to September (and extends up to October in the southernmost parts). Since the basin is characterized by a wider altitudinal gradient (Fig. 1), it exhibits various agro-climatic classes having different amounts of rainfall and temperature. The long term mean annual rainfall ranges from 325 to 1,752 mm (calculated from the merged CHIRPS-gauge product over 37 years 1981–2017).

Agriculture is the dominant economic activity, particularly, in the highlands which receive relatively higher amount of rainfall, rain-fed cereal crop production, mixed farming, and agroforestry-based perennial crop production are the main livelihoods of the inhabitants. The major crops grown in the basin include teff (Eragrostis tef), maize (Zea mays), wheat (Triticum), arabica coffee (*Coffea arabica*) and enset (*Ensete ventricosum*) (USAID, 2012). The lowlands, on the other hand, are characterized by minimal amount of rainfall and dominantly pastoral livelihood. Still in between these two livelihood strategies, the agro-pastoralists rely on a combination of crop production and pastoralism.

2.2. Data sources

In this study, a combination of ground measured datasets and satellite-based rainfall estimates were used. Quality-checked daily rain gauge observations were obtained from the National Meteorological Agency of Ethiopia (NMA). While the open source satellite-based derived CHIRPS monthly rainfall estimates datasets were downloaded from: (ftp://ftp.chg.ucsb.edu/pub/org/chg/products/CHIRPS-2.0/).

2.3. CHIRPS rainfall estimate

The Climate Hazards group Infrared Precipitation with Stations (CHIRPS) is a new quasi-global (50°S-50°N), and high spatial resolution (0.05°) satellite–derived rainfall product. It was primarily developed to support the United States Agency for International Development Famine Early Warning Systems Network (FEWS NET). It is produced from five main data sources (Funk et al., 2015). One of the input data for CHIRPS is the monthly precipitation climatology, CHPClim, temporally disaggregated at each grid cell location into 72 pentads per year (6-pentads per month) long-term average accumulation values. The second source is the quasi-global geostationary thermal infrared (IR) satellite observations from two NOAA sources, the Climate Prediction Center (CPC) IR (with half hour temporal resolution, 4 km spatial resolution, from 2000–present) and the National Climatic Data Center (NCDC) B1 IR (3 h temporal resolution, 8 km spatial resolution, for 1981–2008). The Tropical Rainfall Measuring Mission (TRMM) 3B42 product from NASA to calibrate global Cold Cloud Duration (CCD) rainfall estimates, and atmospheric model rainfall fields from the NOAA Climate Forecast System, version 2 (CFSv2) are also among the main data sources. Finally, as the fifth input data, *in-situ* based measured precipitation data obtained from various sources including national and regional meteorological services are incorporated to produce the CHIRPS rainfall estimates (Funk et al, 2014b, 2015).

2.4. Merging satellite-gauge rainfall data

A technique of merging satellite-gauge rainfall that engage spatial interpolation was adopted by Dinku, Hailemariam (Dinku et al., 2013) in Ethiopia at a national-scale using available data from the rain-gauge stations over the country. A merging technique that involves spatial interpolation strongly demands dense networks of rain gauge-station (Lopez et al., 2015) since rainfall is a spatially variable climate element (Mishra, 2013). However, the study area consists of very sparse and unevenly distributed rain gauge stations, which are inadequate for the application of spatial interpolation. In light of this constraint, instead of adopting a merging technique that involves spatial interpolation, like the one applied by Dinku, Hailemariam (Dinku et al., 2013), a specific

correction factor for each month was used to blend the satellite estimates with the ground-measured rainfall data so as to adjust the bias of the satellite estimates. This temporally variant merging technique was chosen in order to characterize the rainfall climatology of each calendar month.

Accordingly, using a point-to-pixel comparison (Tesfamariam et al., 2019; Ayehu et al., 2018; Dembélé and Zwart, 2016), a bias ratio of the CHIRPS rainfall estimate was first calculated at monthly-scale, separately for each calendar month for 16 years (1990–2005). Then, the mean bias ratio obtained for each month calculated over the calibration period (1990–2005) was used as a correction factor of the respective monthly CHIRPS rainfall estimates. This correction factor was also applied for each respective month, going back and forth of the calibration period for the time before 1990 and after 2005 as applied by Dinku, Hailemariam (Dinku et al., 2013).

Finally, the merged product was validated using temporally independent datasets over five years (2006–2010). For both the merging and validation purposes*, in-situ* rainfall data from 15 rain gauge stations were used. In terms of bias, the validation statistics shows that except for January (having 9% overestimation), the results for the rest of the calendar months were very close to the reference ground measured rainfall, ranging from 3% under-estimation in August (rainy season) to 4% overestimation observed in December (dry season). The relatively higher but still reasonably good bias ratio observed in January and December (both in the dry season of the study area) is perhaps due to the inherent characteristics of the CHIRPS algorithm as it generally overestimates frequency of rainfall, more likely to prevail during the dry season (Tesfamariam et al., 2019; Ayehu et al., 2018; Funk et al., 2015). The method of calculating bias ratio was adopted from earlier validation studies (Dinku et al., 2008; Tesfamariam et al., 2019; Ayehu et al., 2018; Toté et al., 2015; Dembélé and Zwart, 2016) as mathematically expressed below.

$$\text{Bias} = \frac{\sum_{i=1}^{n} S_i}{\sum_{i=1}^{n} G_i} \tag{2.1}$$

Where: G_i = gauge rainfall measurements, and S_i = satellite rainfall estimate

2.5. Variability and trend analyses of rainfall and temperature

Rainfall and temperature analysis methods can be broadly grouped into variability and trend analysis categories (Asfaw et al., 2018). Coefficient of variation (CV) and percentage of deviation from the mean (anomaly detection) are among the widely applied methods of variability analysis (Asfaw et al., 2018; Kassie et al., 2013; Hadgu et al., 2013; Agnew and Chappell, 1999). Similarly, trend analysis of rainfall and temperature can be performed using parameteric and non-parametric tests. Unlike parametric methods, non-parametric tests are more flexible as they do not depend on normally distributed time series data (Gilbert, 1987). As a result, the non-parametric method, Mann–Kendall trend test is widely applied regardless of the normality of the input data distribution (Mohammed et al., 2017; Degefu and Bewket, 2014; Asfaw et al., 2018; Kassie et al., 2013; Chattopadhyay and Edwards, 2016). Accordingly, Mann–Kendall trend test (Kendall, 1975; Mann, 1945) and Sen's slope estimator (Sen, 1968) were used in this study in order to detect trends in the time series rainfall and temperature data. Weather stations having greater than 30 years of time series rainfall and temperature records were used for the trend analysis (Table 1). Thus, Mann–Kendall trend test was calculated using the following procedures according to Gilbert (1987)

$$S = \sum_{i=1}^{N-1} \sum_{j=i+1}^{N} \text{sgn}(x_j - x_k) \tag{2.2}$$

Where S indicates the number of positive differences minus the number

Table 1
Name and location of weather stations used for trend analysis.

Station name	Long.	Lat.	Elevation	Time (years)	Agroecology
Awassa	38.48°	7.07°	1694	1980–2016	*Weyna Dega*
Arbaminch	37.56°	6.06°	1207	1987–2016	*Kolla*
Billate	38.08°	6.82°	1361	1985–2016	*Kolla*
Konso	37.43°	5.33°	1431	1987–2016	*Kolla*
Kulumsa	39.16°	8.01°	2211	1980–2016	*Weyna Dega*
Ziway	38.70°	7.93°	1640	1982–2016	*Weyna Dega*

of negative differences and N stands for the number of data points (Gilbert, 1987); X_j and X_k are the monthly values in successive years of j and k, $j > k$.

sgn $(X_j-X_i) = 1$, if $X_j-X_k > 0$, $= 0$, if $X_j-X_{k=} 0$, and $= -1$, if $X_j-X_k < 0$

Likewise, the variance of S was computed using the following equation which also takes into account tied values (equal values) that mat be present in the time series (Gilbert, 1987).

$$VAR(S) = \frac{1}{18}\left[n(n-1)(2n+5) - \sum_{p=1}^{q} t_p(t_p-1)(2t_p+5) \right] \quad (2.3)$$

Where q is the number of tied groups and t_p is the number of data in the pth group.

Then the S and VAR(S) were used to compute the standardized test statistic Z as follows:

$$Z = \frac{S-1}{[VAR(S)]^{1/2}}, \text{ if } S > 0 \quad (2.4)$$

$$Z = 0, \text{ if } S = 0$$

$$Z = \frac{S+1}{[VAR(S)]^{1/2}}, \text{ if } S < 0$$

A positive (negative) value of Z indicates an upward (downward) trend, respectively (Gilbert, 1987).

On the other hand, to understand the degree of rainfall variability, coefficient of variation (CV) and standardized rainfall anomaly (SRA) were used. Both the CV and SRA were calculated from the blended satellite-gauge product and the analysis was performed on agroecological basis as well as for the whole basin. The coefficient of variation (CV) was computed and mapped for the annual and wet season rainfall. It was calculated as used by Kassie, Rötter (Kassie et al., 2013) and Asfaw, Simane (Asfaw et al., 2018).

$$CV = \frac{\delta}{\mu} \text{ X } 100 \quad (2.5)$$

Where CV is the coefficient of variation; δ is the standard deviation and μ is the mean precipitation over the period of observation (1981–2017).

Similarly, a standardized rainfall anomaly (SRA) was computed using the area average rainfall of the whole basin and major agroecological zones at annual and seasonal temporal scales. The SRA was calculated according to Agnew and Chappell (1999).

$$SRA = \frac{X_i - \mu}{\delta} \quad (2.6)$$

Where SRA is standardized rainfall anomaly; X_i is the annual/seasonal rainfall of a particular year; μ is the mean and δ is the standard deviation of the annual/seasonal rainfall over 30 years (1981–2010). Standardized rainfall anomaly is useful in detecting dry and wet years in the time series which also enables to assess the frequency and severity of meteorological droughts (Agnew and Chappell, 1999).

2.6. Computing standardized precipitation index

The Standardized Precipitation Index (hereafter SPI) was adopted in the present study, as a measure of drought intensity at relevant time-scales (McKee et al., 1993). This drought index (SPI) demands time series monthly precipitation data for at least 30 years (WMO, 2012; McKee et al., 1993). Although it depends on a single meteorological element, precipitation, SPI is a powerful and flexible index for evaluating meteorological drought (Guttman, 1998). Unlike the Palmer Drought Severity Index, SPI is spatially consistent as it is a standardized transform of the probability of observed precipitation data (Guttman, 1998). Moreover, SPI is just effective for analyzing wet periods as it is for dry periods (WMO, 2012; Guttman, 1998). Accordingly, in this study, pixel-based SPI values were calculated using the time series rainfall data of the merged satellite-gauge rainfall product. This merged product was chosen so as to assess the spatial extent of drought events across AEZ in the basin. It was calculated for 37 years (1981–2017) at 3-month and 4-month timescale representing the rainy seasons locally known as *Belg* (March–May) and *Kiremt* (June–September), respectively. These seasons were chosen for drought characterization because both seasons in combination contribute greater than 70% of the annual climatological mean rainfall of the study area.

Calculating SPI requires fitting a gamma probability density function to a given frequency distribution of precipitation totals for a station as Thom (1966) found that the gamma distribution very well fits climatological precipitation time series data. According to McKee, Doesken (McKee et al., 1993), the gamma function is mathematically expressed as:

$$g(x) = \frac{1}{\beta^{\alpha}\Gamma(\alpha)} x^{\alpha-1} e^{-x/\beta}, \text{ for } x > 0 \quad (2.7)$$

Where: $\alpha > 0$, is a shape parameter; $\beta > 0$, is a scale parameter; $x > 0$, is the precipitation amount and $\Gamma(\alpha) = \int_0^{\infty} y^{\alpha-1} e^{-y} dy$, is the gamma function

The cumulative probability of precipitation is computed as:

$$G(x) = \int_0^x g(x)dx = \frac{1}{\widehat{\beta}^{\widehat{\alpha}} \Gamma(\widehat{\alpha})} \int_0^x x^{\widehat{\alpha}-1} e^{-x/\widehat{\beta}} dx \quad (2.8)$$

To accommodate zero values of the precipitation distribution since the gamma function is undefined for $x = 0$, the cumulative probability becomes:

$$H(x) = q + (1 - q) G(x) \quad (2.9)$$

Where q is the probability of a zero precipitation.

Finally the cumulative probability, H(x) is transformed to the standard normal distribution with mean of zero and variance of one to produce the SPI (McKee et al., 1993), which is conceptually equivalent to the *Z*-score used in statistics and calculated as:

$$SPI_{ij} = \frac{X_{ij} - \mu_{ij}}{\alpha_{ij}} \quad (2.10)$$

Where SPI_{ij} is the SPI of the ith month at the jth timescale, X_{ij} is precipitation total for the ith month at the jth timescale, μ_{ij} and σ_{ij} are the long-term mean and standard deviation associated with the ith month at the jth timescale, respectively.

Pixel-based or continuous SPI using the blended satellite-gauge product was calculated using the SPIRITS Software version 1.5.2, which is an open source software developed by the VITO (Eerens and Haesen, 2016).

Generally, variability and trend analysis of rainfall and temperature as well as drought assessment was carried out on agroecological basis as rainfall and temperature variability is strongly linked to agroecological differences (Hurni, 1998).

3. Results

3.1. Agroecological classification of the study area

Agroecological zonation can be defined as the spatial classification of a landscape into relatively similar agricultural and ecological characteristics (Hurni, 1998), which provides a framework to understand the complexity of agroecosystems (Altieri, 1995). In mountainous countries like Ethiopia where the most prominent mountain system in Africa is found, topography plays an important role in agroecological zonation (Hurni, 1998). Accordingly, the elevation-based agroecological zonation developed by Hurni (1998) was adopted in this study to classify the basin into six agroecological zones (AEZs). According to the same author these AEZs are locally named as *Berha* (<500 m.a.s.l), *Kolla* (500–1500 m.a.s.l), *Weyna Dega* (1500–2300 m.a.s.l), *Dega* (2300–3200 m.a.s.l), *High dega*(3200–3700 m.a.s.l), and *Wurch* (>3700 m.a.s.l) (Fig. 2). This classification was performed using a 30 m spatial resolution SRTM DEM due to its good vertical and horizontal accuracy (Luana et al., 2015; NASA and Overview of SRTMASTER DEM Data, 2017).

Agroecological zonation, is typically important to improve planning of agricultural development as agroecological zones strongly relate to climatic parameters such as rainfall amount and variability, temperature, and vegetation characteristics (Hurni, 1998). In this context, it is important to understand the long term rainfall and temperature variability as well as the subsequent drought events across the major agroecological zones in the study area. Subsequently, it helps to identify the most drought affected agroecological zones, which may in turn enable decision makers to design ecologically sound drought adaptation strategies. To this end, analysis of rainfall and temperature variability was performed on the three major AEZs in the basin (*Kolla, Weyna Dega* and *Dega*) which in combination covers more than 97% of the basin's surface area (Fig. 2). These AEZs (*Kolla, Weyna Dega* and *Dega*) are also important from agricultural point of view as they are suitable for most of the cereal crops grown in Ethiopia (Hurni, 1998).

3.2. Annual and seasonal rainfall distribution across agroecological zones

Understanding climatological mean rainfall distribution across agroecologies especially in the bimodal rainy seasons enables to identify areas experiencing continuous moisture stress. The *Belg* and *Kiremt* seasons generally control agricultural production the country as well as in the study area. For example, the spring or *Belg* rain essentially determines availability of pasture and water for livestock in the pastoral lowlands of the study area. This season is also useful for crop production as many farmers plant slowly maturing long cycle crops that grow during both the *Belg* and *Kiremt* seasons (Viste et al., 2013; USAID,

2012). More importantly, the *Kiremt* rain significantly controls crop production in larger part of the study area.

The mean annual and seasonal rainfall distribution in the basin shows that the highland agroecologies (*Weyna Dega*, *Dega*, and High *Dega*) receive higher amount of rainfall than the adjacent lowlands (Fig. 3). As the study area is characterized by a wider altitudinal range (Fig. 1), the difference in the spatial distribution of rainfall amount could be attributed to orographic nature of rainfall (Viste et al., 2013; Dinku et al., 2007). Furthermore, the spatial distribution of rainfall amount in the study area exhibits seasonal differentiation (Fig. 3). For instance, the northern half receives higher amount of rainfall during the *Kiremt*, confirming that *Kiremt* is the main rainy season in this part of the basin. In the *Kiremt* season, rainfall amount declines gradually southward with the southernmost receiving the lowest amount. On the other hand, the southern half receives relatively higher amount of rainfall during the Belg, which is known to be the main rainy season in the southern part (Fekadu, 2015; Viste et al., 2013; Degefu and Glantz, 1987). However, even in the *Belg* season, large area of the southern lowlands (*Berha* and *Kolla* agroecologies) receive very low amount of rainfall compared to the other agroecologies (Fig. 3). Area average climatological mean annual rainfall of the major agroecologies are also given below.

The annual mean rainfall pattern (Fig. 4) clearly shows the effect of elevation in determining rainfall amount. As a result, the *Dega*, *Weyna Dega*, and *Kolla* agroecologies receive the highest, intermediate and lowest amount of mean annual rainfall, respectively, following their sequence of altitudinal gradients (Fig. 4). This shows a strong correlation between rainfall amount and elevation range.

3.3. Inter-annual and seasonal variability of rainfall

Coefficient of variation (CV) and standardized rainfall anomaly (SRA) were used to analyze and unerstand the degree of rainfall variability in the study area. These are usefull and widely accepted measures of rainfall varibility (Asfaw et al., 2018; Kassie et al., 2013; Hadgu et al., 2013; Agnew and Chappell, 1999). The coefficient of variation (CV) was computed on a pixel by pixel basis for the whole basin particularly for the annual and wet season rainfall totals (Fig. 5).

As used by Asfaw, Simane (Asfaw et al., 2018), the rainfall coefficient of variation is categorized as less (CV< 20%), moderate (20% < CV<30%), and high (CV>30%). In this context, rainfall in the *Belg* and *Kiremt* seasons has exhibited higher coefficient of variation (CV) than the annual total, with further higher magnitudes in the *Kiremt* but larger areal extent in the *Belg* season (Fig. 5). While the maximum CVs of the *Belg* and Kiremet rainfall reaches the maximum range (CV>30%), the highest CV of the annual rainfall is limited to the moderate category (CV<30%). As far as agroecology is concerned, the inter-annual variability of *Kiremt* rainfall in terms of CV is low in the *Weyna Dega*, *Dega*, and *high dega*agroecologies of the northern parts, where *Kiremt* is the main reason. Thus, the annual crop growing areas in the northern part of the basin are characterized by a low inter-annual variability of *Kiremt* rainfall (with CV < 20). The highest CV in this season mainly lies in the pastoral areas of the *Kolla* and *Berha* agroecologies of the southernmost part, which receive the lowest amount of annual rainfall in the basin.

On the other hand, the *Belg* rain has exhibited moderate inter-annual variability in terms of CV across all agroecologies in larger part of the study area. It was found to be equally variable even in the southern parts where *Belg* is the main rainy season (Fig. 5). Overall, the marked difference in the CVs especially in the rainy seasons shows a considerable spatial variability of rainfall across AEZs. Most importantly, the maximum spatial variability in each timescale (inter-annual, *Kiremt*, and *Belg* seasons rainfall) lies in the low rainfall areas of the southern lowlands (Fig. 5). In turn, this indicates higher vulnerability of the southern lowlands to drought incidences implying direct impact on livestock rearing, the main economic activity in this part.

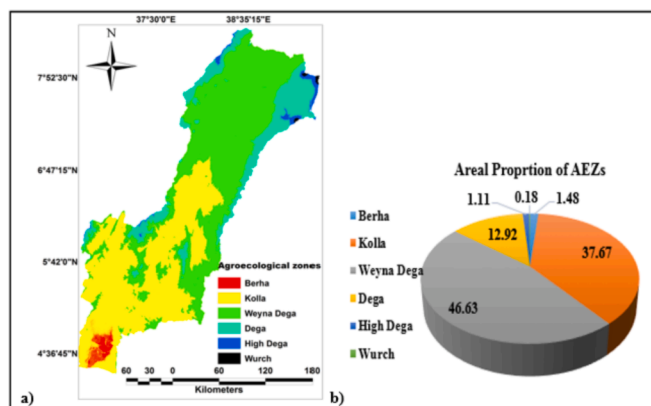In addition to coefficient of variation, area average-based

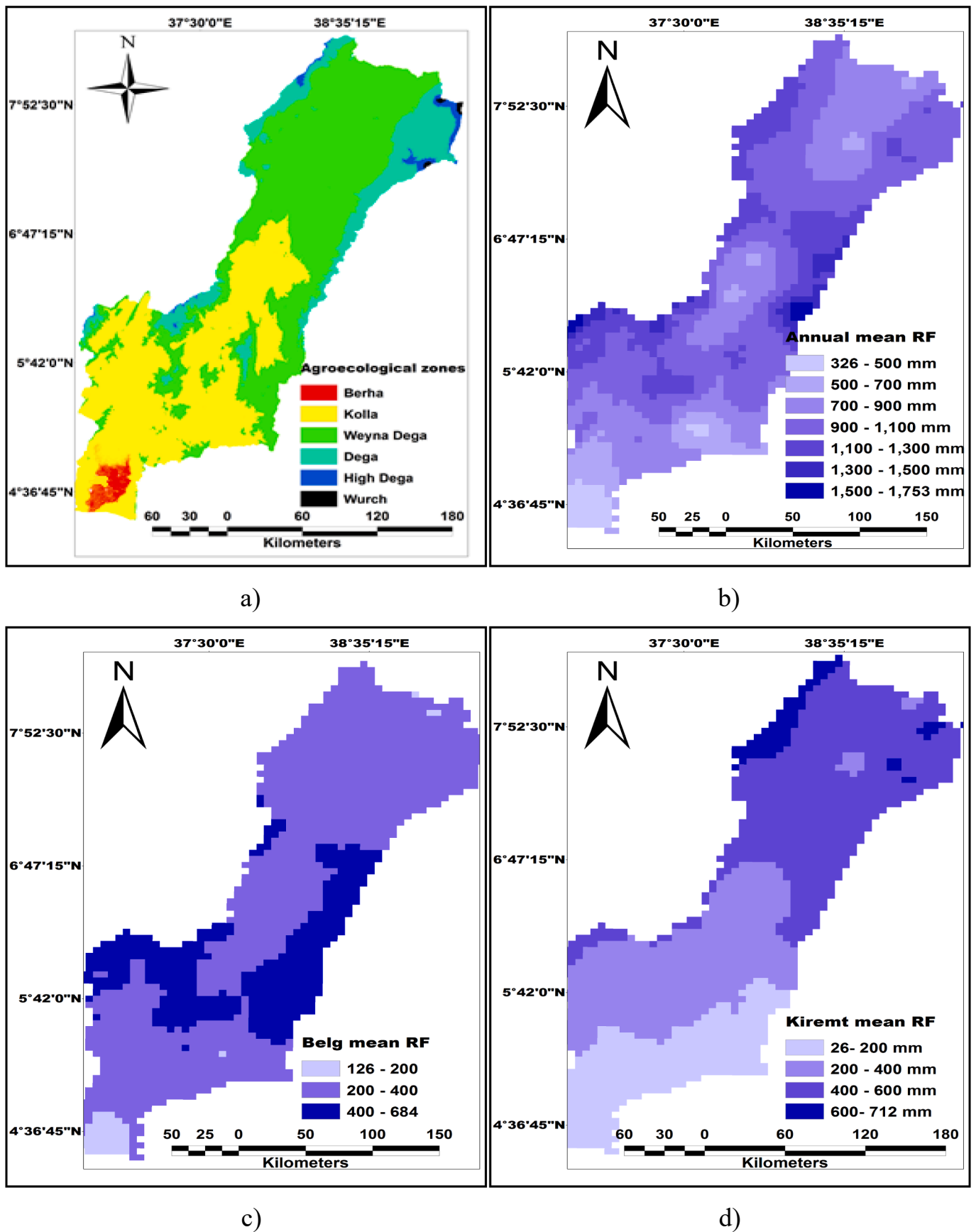**Fig. 2.** Agroecological classes of the rift valley lakes basin a) Location, b) Proportion.

Fig. 3. Distribution of mean rainfall across AEZs: a). Map of agroecological zones b) Mean annual rainfall (1981–2017) c) Mean *Belg* season rainfall (1981–2017), d). Mean *Kiremt* season rainfall (1981–2017).
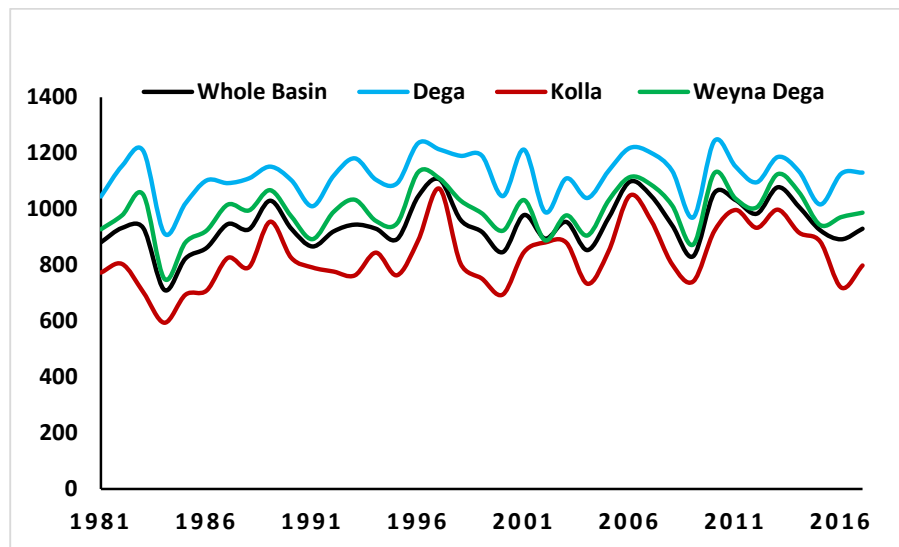
Fig. 4. Patterns of areal mean annual rainfall in the rift valley lakes basin and major AEZs (1981–2017) (*Note: Areal mean rainfall is the sum of the rainfall value of each pixel divided by the total number of the pixels in the basin and/or each AEZ).

standardized rainfall anomaly (SRA) was also used to assess further rainfall variability in the basin. It was carried out for the whole basin as well as the major agroecologies (*Kolla, Weyna Dega* and *Dega*) at annual and seasonal temporal scales. Following Agnew and Chappell (1999), area average-based SRA was calculated over 37 years (1981–2017) against the 1981–2010 the annual and seasonal mean raifall of the Rift Valley Lakes Basin (RVLB) and each agroecology zone. The area average rainfall was chosen to compute annual and seasonal SRAs as the aim of this statistical indicator was to detect the dry and wet years and their frequency in the time series data thereby to understand the annual and seasonal rainfall variability in the basin.

The results of the standardized rainfall anomalies were assessed according to the drought classification scale of Agnew and Chappell (1999), who have categorized SRA values as extreme drought (SRA < −1.65), severe drought (−1.28 > SRA > −1.65), moderate drought (−0.84 > SRA > −1.28), and no drought (SRA > −0.84). According to this drought classification, the SRAs designating extreme and severe drought years were less frequent compared to the documented drought years in the country (Mohammed et al., 2017; Degefu and Bewket, 2014). This is reasonably due to the smoothing (averaging) effect since the SRA was calculated for the area average rainfall of the whole basin and each agroecology zone. However, the negative anomalies designating drought years (SRA < −0.85) were able to reveal the major historical drought periods. For instance, at the annual scale, over the basin and the AEZs, less than −0.85 SRAs were found for the major drought years in 1984, 1991, 2000, 2002, and 2009 (Mohammed et al., 2017; Degefu and Bewket, 2014).

In addition to the magnitude and frequency of rainfall anomalies, it is also important to understand the temporal patterns of the deviations in the time series. Thus, while differences exist between agroecologies, the frequency of negative anomalies (dry years) especially at the annual and the *Kiremt* season was relatively higher in the 1980s followed by the 1990s. Whereas the positive anomalies (wet years) were more frequent mainly after 2000s (Fig. 6). The declining trend in the frequency of negative departures could indicate a corresponding decline in drought frequency.

On the other hand, in the *Belg* season, although rainfall irregularities are evident, the deviations did not exhibit a distinct temporal pattern as the negative and positive rainfall deviations were almost uniformly distributed in the time series except for the *Kolla* AEZ. Whereas at the *Kolla* AEZ, more negative anomalies (dry periods) were observed in the 1980s and 1990s while more positive anomalies (wet periods) were

found in the 2000s (Fig. 7). This distinction could be associated to the seasonal differentiation of rainfall since the *Belg* is the main rainy season only in the southern part of the basin mainly chracterized by the *Kolla* AEZ (see Fig. 8).

Unlike the case in the *Belg,* the temporal patterns of rainfall deviations in the *Kiremt* season were found to be similar to the annual deviations as the frequency of negative deviations in both times were higher during the 1980s and 1990s while positive deviations were more frequent in 2000s across all AEZs. Furthermore, in this season, narrow range deviations were observed in the *Kolla* AEZ especially in the 1980s and 1990s. As *Kiremt* is not the main rainy season in this AEZ due to its location in the southern part of the basin (Fig. 2), the *Kolla* AEZ receives generally low amount of rainfall in this season. Its climatological mean *Kiremt* season rainfall (over 1981–2010) is 207.18 mm, by far lower than the corresponding 513.86 mm and 411.07 mm for the *Dega* and *Weyna Dega* AEZs, respectively. As a result, the narrow range anomalies observed in the *Kolla* AEZ may not be due to rainfall consistency; rather it could be associated to the inherently low amount of rainfall during the *Kiremt* season.

Generally, rather than areal averages, using rainfall values of each pixel is more informative of drought events and their spatial distributions. However, the irregularities observed in the annual and seasonal rainfall, particularly the substantial number of negative anomalies across all AEZs in the basin could be generally associated with high probabilities of drought occurrence.

3.4. Trends of rainfall and temperature

Trends of time series mean monthly minimum, mean monthly maximum, and mean monthly air temperatures as well as monthly, seasonal and annual rainfall totals were analyzed. Thus, six meteorological stations for rainfall and five stations for temperature with greater than 30 years of time series data were analyzed for trend test (Table 1).

The Mann-Kendall trend values for the monthly, seasonal, and annual rainfall totals show that only few months have undergone statistically significant trends at 50% of the stations (Table 2). Accordingly, at the monthly timescale, significant decreasing trends were found at Billate station in December; and at Konso station in January. Whereas significant increasing trends were observed at Billate, and Konso stations in November; and at Ziway station in June and July months. In contrast, no significant trend was found for the annual, *Belg* season (March–May) and *Kiremt* season (June–September) rainfall in either of the stations.
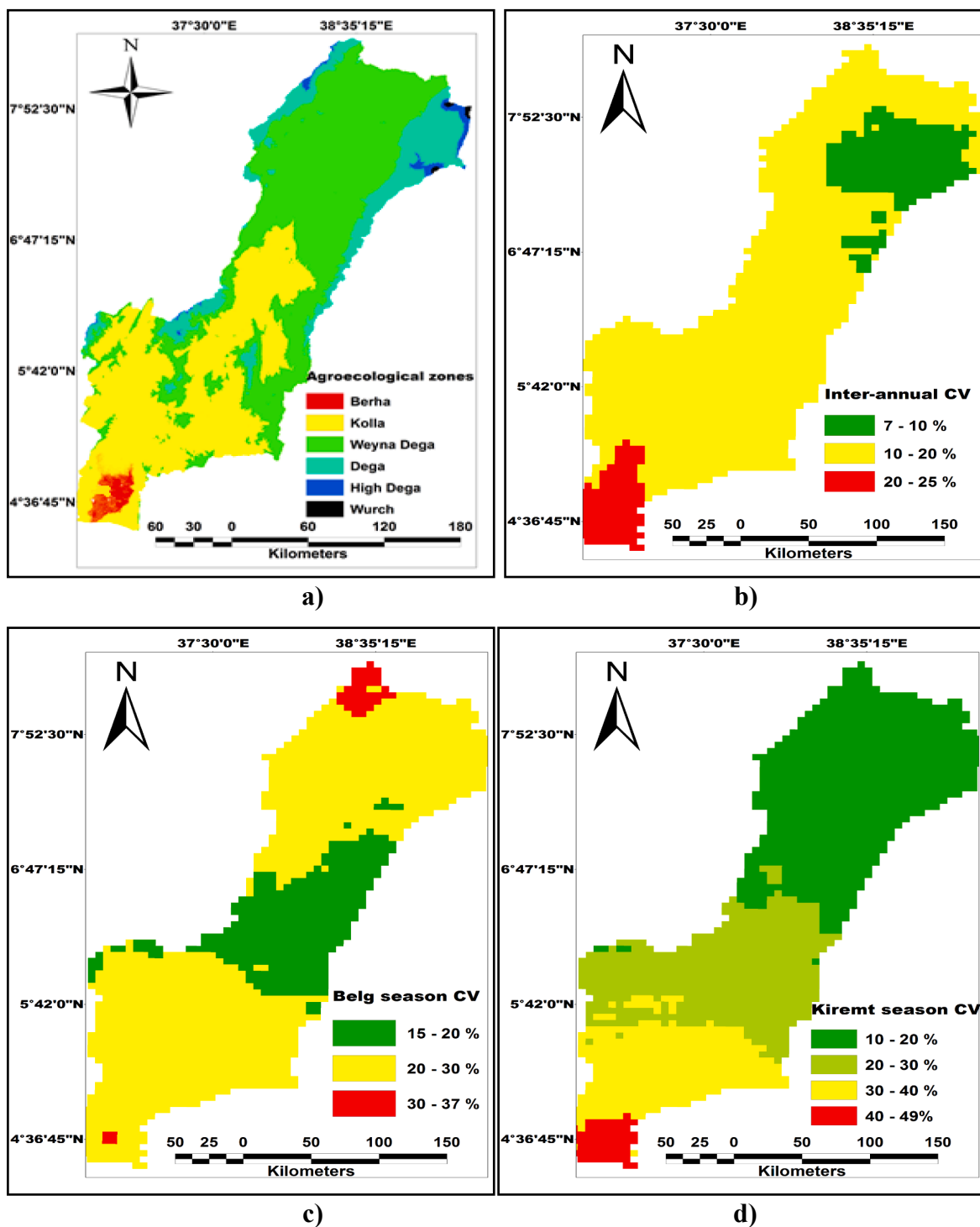
Fig. 5. Rainfall coefficient of variation (CV) across AEZs: a). Agroecological zones b) Inter-annual rainfall CV (1981–2017) c) *Belg* season rainfall CV (1981–2017), d) *Kiremt* season rainfall CV (1981–2017).

Similarly, Kassie, Rötter (Kassie et al., 2013) have reported a non-significant decline in the annual*, Belg,* and *Kiremt* rainfall for Ziway, Awassa, and Kulumsa stations. Generally, while the significant declining trends were found to be rare, a declining tendency was observed in 39% and 50% of the months constituting the *Belg* and *Kiremt* seasons, respectively across all stations (Table 2). In this context, although the impact of this declining tendency seems insignificant currently, a further rainfall decline in the future could have nontrivial impact on the rain-dependent agriculture in the basin.

Unlike the rainfall trends, the Mann–Kendall trends for temperature shows more significant changes. This was exhibited by significant rising trends in monthly minimum, maximum, and mean temperatures in several months at all the five stations (Fig. 9). For instance, 16.67% of the months at Arbaminch station, 33.3% at Ziway, 41.67% at Kulumsa, and 58.33% of the months at Awassa station have experienced statistically significant increasing trend in mean monthly maximum temperature at α 0.05 significance level (Fig. 9). Similarly, Kassie, Rötter (Kassie et al., 2013) have reported significant increasing trends in minimum and
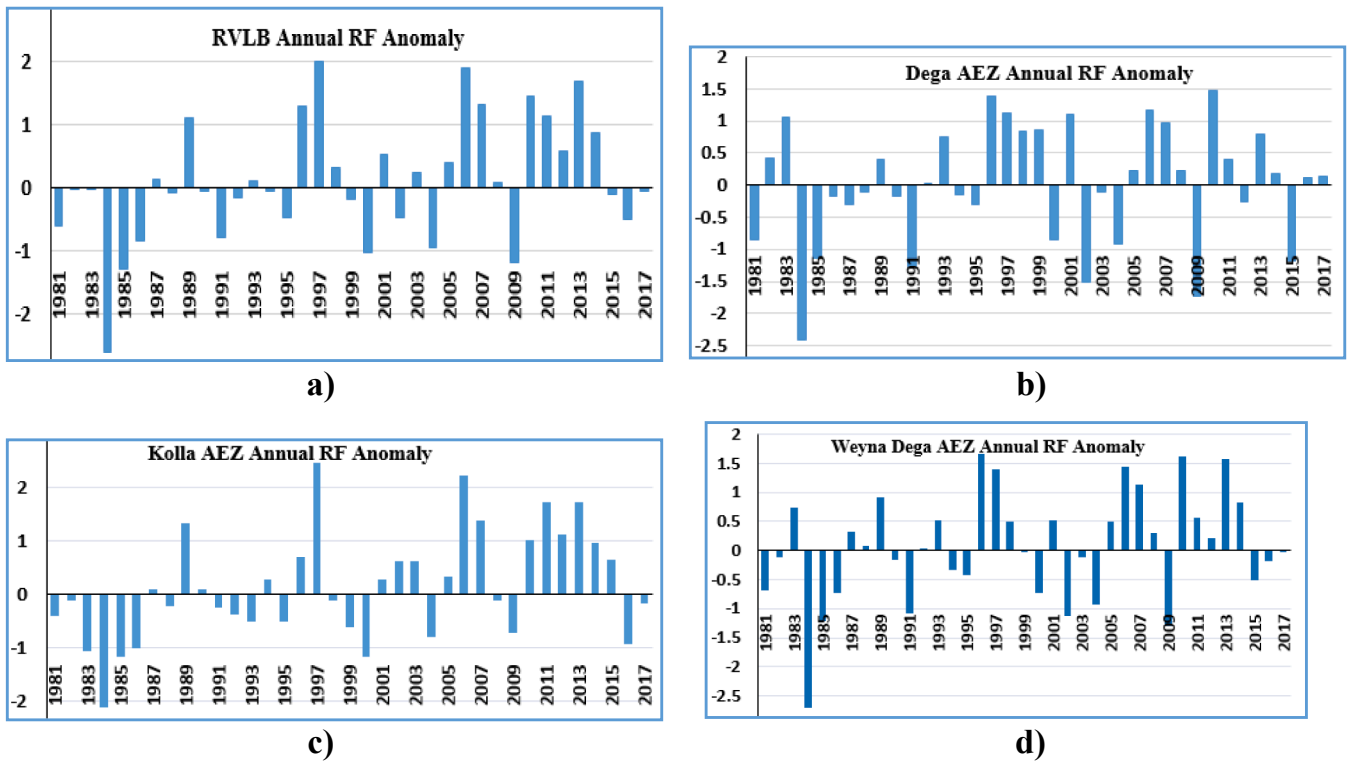
Fig. 6. Annual rainfall anomalies: a) Rift Valley Lakes Basin (RVLB), b) *Dega* AEZ, c) *Kolla* AEZ, d) *Weyna Dega* AEZ.
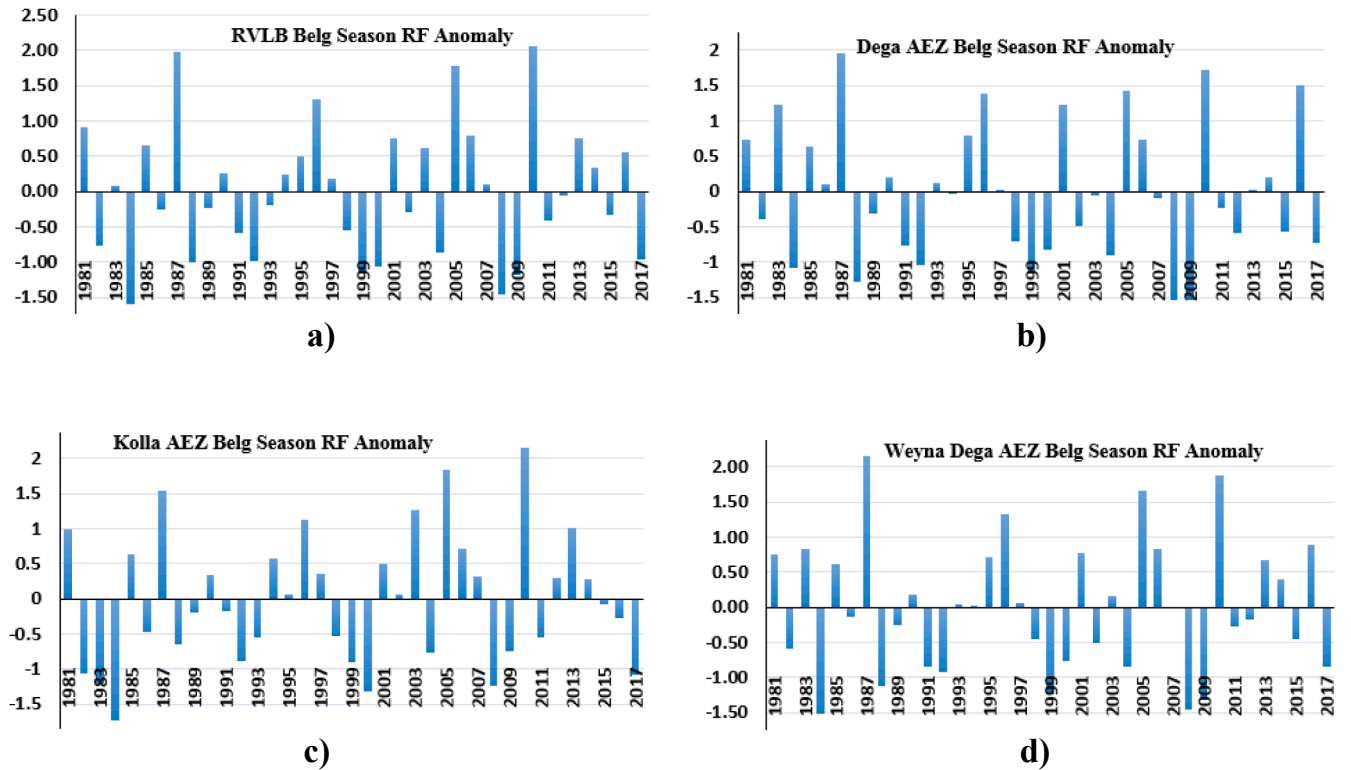

Fig. 7. *Belg* season rainfall anomalies: a) Rift Valley Lakes Basin (RVLB), b) *Dega* AEZ, c) *Kolla* AEZ, d) *Weyna Dega* AEZ.

maximum temperatures for the *Belg* season at Awassa and Ziway stations. More importantly, majority of the months with rising temperatures constitute the rainy seasons, agriculturally crucial time for rain-fed crop production. Consequently, increased warming in the growing seasons obviously leads to a higher rate of evapotranspiration which could cause adverse effects on the rain-fed crop growth. On the other hand, although declining trends in monthly temperatures were observed in some months, none of them was statistically significant at α 0.1
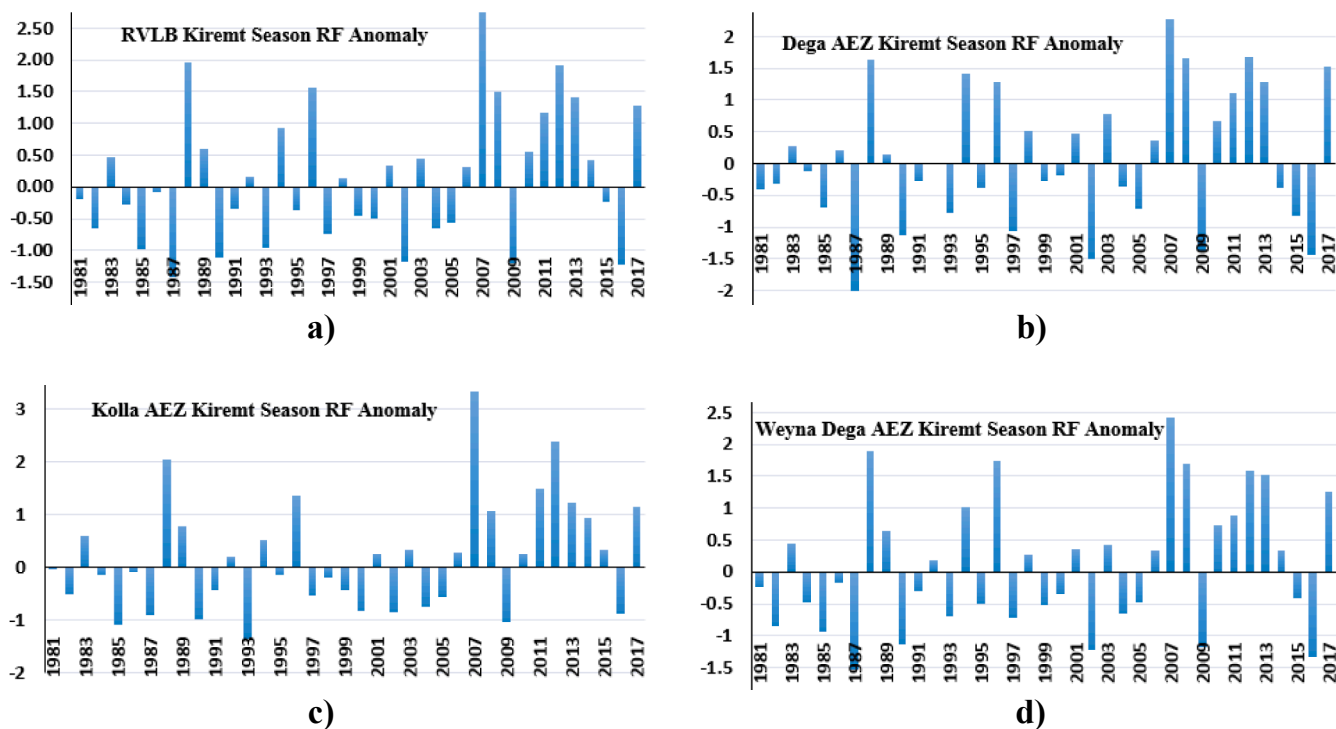
Fig. 8. *Kiremt* season rainfall anomalies: a) Rift Valley Lakes Basin (RVLB), b) *Dega* AEZ, c) *Kolla* AEZ, d) *Weyna Dega* AEZ.

Table 2
Mann–Kendall trend values of rainfall at monthly, seasonal and annual timescales.

Months	Weather stations					
	Awassa	Arbaminch	Billate	Konso	Kulumsa	Ziway
January	0.68	−1.38	0.24	**−2.18****	1.26	0.77
February	−1.19	−1.36	−1.63	−0.70	−1.02	−1.14
March	−0.63	0.45	−0.96	−0.61	−0.43	0.04
April	−0.84	0.07	0.34	0.00	−0.39	0.07
May	0.61	0.23	0.73	0.46	−0.09	−0.12
June	−0.56	1.20	−0.21	0.62	0.80	**1.75***
July	−0.03	−1.04	0.24	0.23	−0.21	**2.16****
August	0.00	−0.30	−0.10	0.79	0.23	−0.79
September	0.03	1.09	0.24	0.61	−1.47	1.12
October	−0.20	0.84	0.71	−0.16	0.79	−0.87
November	1.05	1.59	**1.95***	**2.95****	1.00	1.60
December	0.53	−0.39	**−2.41****	−0.29	−0.28	1.35
Belg season (March-May)	−0.97	0.48	0.15	−0.11	−0.79	−0.45
Kiremt season (June-Sept)	−0.07	0.98	0.79	1.46	0.96	1.11
Annual rainfall	−0.43	1.16	0.28	0.50	−0.54	0.79

Note: * and ** statistically significant at α 0.1 and 0.05 level of significance, respectively.

significance level.

Inter-comparison of the five weather stations considered in this study shows that Awassa station has experienced rising temperature trends in more number of months than the other stations. For instance, this station has experienced statistically significant increasing trends in mean monthly temperature in all the 12 months (at α 0.05 for the 11 months and at α 0.1 for the remaining one month). Similar rising trends were also observed for the monthly minimum and maximum temperatures at this station. This increased rising trends could be related to the phenomenon of 'urban heat island' since the station is located at the center of the Hawassa city. Because this city is one the most rapidly growing urban centers in Ethiopia. Related to this, it was also reported that the city has undergone a significant decline in green area over the last four decades from 30% in 1975 to 12% in 2015 (Molla et al., 2018). Thus, in addition to global warming, the decline in the green area of the city might have some contribution to this increased warming trend. This

warming trend could also accelerate the evaporation rate of Lake Hawassa, surrounding the city, an essential rift valley lake from ecological, hydrological, and economic perspectives. Therefore, effective implementation of urban greenery could be potentially important to modulate the microclimate of rapidly growing urban areas.

3.5. Spatial distribution and intensity of meteorological drought events

As discussed above, the results of variability and trend analysis of rainfall in the basin has exhibited great variations across agroecologies. Consequently, pixel-based SPI was computed to assess the intensity and spatial distribution of meteorological drought events in the basin. Thus, drought intensities were categorized according to Hayes (Hayes, 1994–2001) who has condensed the four categories of McKee, Doesken (McKee et al., 1993) into three classes by merging the 'mild drought' into a 'near normal' category. These drought intensities were
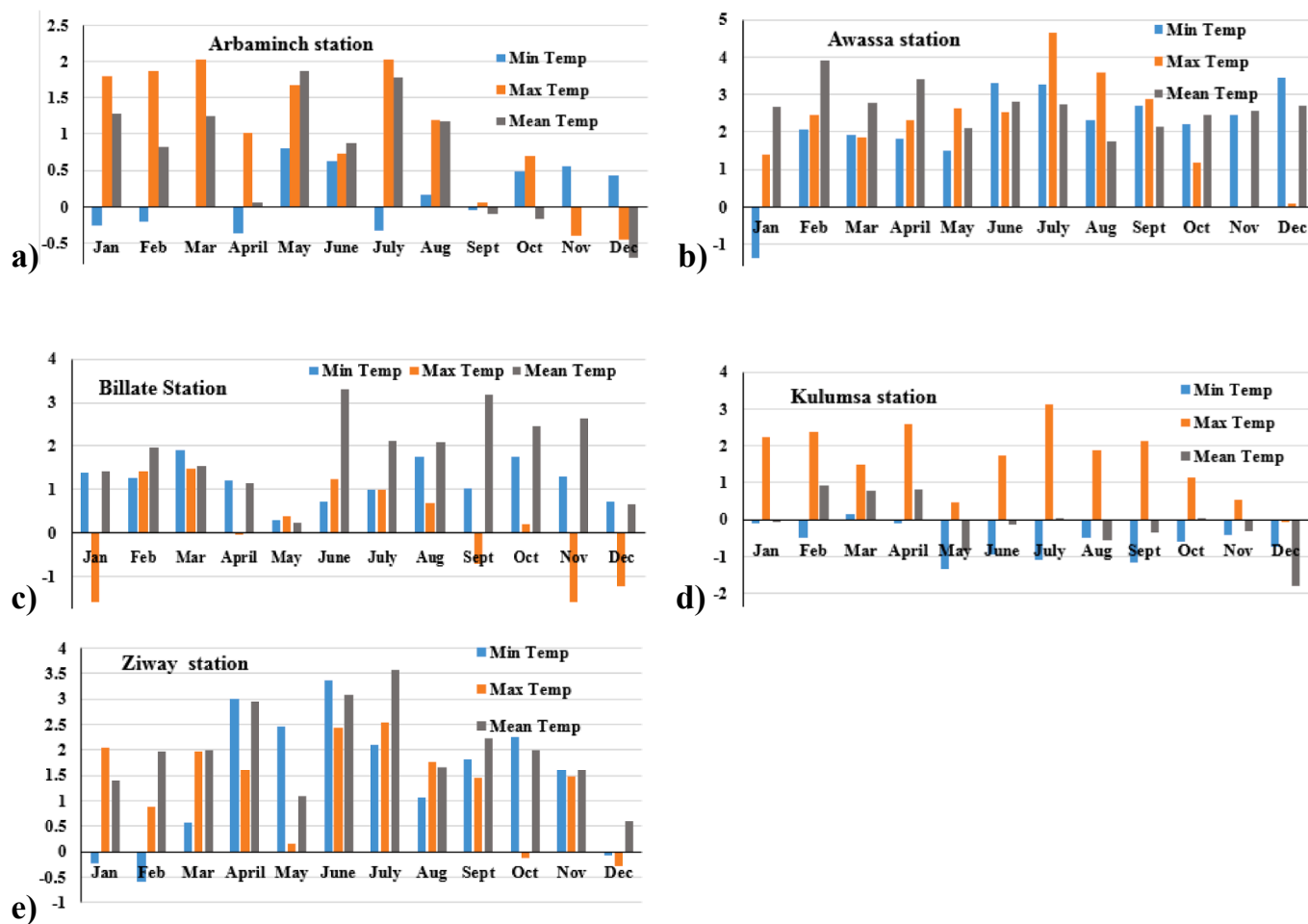
Fig. 9. Mann–Kendall trend Z score values of mean monthly, mean monthly minimum, and mean monthly maximum air temperatures: a) Arbaminch station, b) Awassa, c) Billate, d) Kulumsa, and e) Ziway stations.

moderately dry, severely dry, and extremely dry (Table 3). These categories were adopted in order to focus on the higher intensities of drought events following the work of Degefu and Bewket (2014).

The drought assessment was performed primarily focusing on the bi-modal rainy seasons, *Belg* (March–May) and *Kiremt* (June–September) following the works of Viste, Korecha (Viste et al., 2013) and (Mohammed et al., 2017). Because, there is a strong dependence on the rain that falls during these seasons for rain-fed agriculture, in the basin and generally in the country (Viste et al., 2013; USAID, 2012; Funk et al., 2015). In the study area, the average contribution of the *Belg* and *Kiremt* rain to the annual mean exceeds 70% (Fig. 3). As a result, failure of the expected rainfall in these growing seasons leads to drought incidences.

In both rainy seasons, the variability and irregularity of rainfall in the basin has subsequently resulted in frequent drought episodes with varying intensity. Besides, the location and spatial distribution of the

Table 3
SPI values and corresponding drought intensity categories (Hayes, 1994–2001).

SPI values	Drought Intensity
≥2	Extremely wet
1.5 to 1.99	Very wet
1 to 1.49	Moderately wet
−0.99 to 0.99	Near normal
−1 to −1.49	Moderately dry
−1.5 to −1.99	Severely dry
< -2_____	Extremely dry_____

historical drought events in the study area shows that different agro-ecological zones were affected in different times (Fig. 10 and 11). The temporal correspondence of the historical droughts occurred in the study area was compared with the documented major national drought years in the country. Accordingly, most of the historical drought episodes the study area has experienced in the bimodal rainy seasons correspond to the documented historical droughts events in the country. Specifically, the SPI maps have revealed the most disastrous drought hazards particularly occurred in the southern parts of the country as compiled by Degefu and Bewket (2014), and Mohammed, Yimer (Mohammed et al., 2017). For example, a direct correspondence was observed in both the *Belg* and *Kiremt* seasons to the drought events occurred in the country in 1982, 1983–84, 1988, 1987–1988, 1991–1992, 1993–1994, 2000, 2002–2003, 2008–2009, 2011, and 2015–2016 (Fig. 10 and 11). As a result, its ability to retrieve the recognized historical drought events indicates the reliability of the merged satellite-gauge rainfall product used to compute the drought index in this study.

Furthermore, in addition to the registered droughts years which were common to the study area and other parts of the country, more drought episodes were observed particularly in the study area, at 3-month SPI in the *Belg* and at 4-month SPI in the *Kiremt* seasons. These drought years were in 1981, 1985,1989, 1990, 1995, 1997, 1999, 2001, 2004, and 2014 at the 3-month SPI in the *Belg* and in 1981, 1985, 1986, 1990, 1995, 1996, 1998, 2001, 2005, and 2010 at the 4-month SPI in the *Kiremt* season. Among these, extreme and severe droughts in 1981, 1990, and 1999 in the *Belg;* 1985 and 1990 in the *Kiremt* seasons have

affected large portions of the study area (Fig. 10 and 11). For instance, the area affected by extreme drought intensity in 1981 during the *Belg* season was 24.33% of the total area, larger than the area affected during the 1984 devastating national drought (Fig. 10). This drought year, however, was not nationally recognized as a major drought period. Of course, some drought episodes registered in other parts of the country were not observed in the study area. However, these are fewer in number. This clearly indicates that the study area is highly vulnerable to frequent drought events although it varies across agroecological zones. As a result, partially, the basin has experienced at least a moderate drought intensity, on average every 1.68 years in the *Belg* and 1.76 years interval in the *Kiremt* seasons during the 1981–2017. More importantly, in the *Kolla* AEZ, higher coefficient of rainfall variation and higher frequency of drought events than the highland AEZs were observed (see Fig. 11).

4. Discussion

A high variability of rainfall was observed in the study area in terms of amount and spatiotemporal distributions and subsequently resulted in frequent drought episodes with varying intensities both in the *Belg* and *Kiremt* seasons. This rainfall variability could be attributed to various factors of local and global nature. To some extent, the spatio-temporal rainfall variability might be due to the effects of local topography, as the study area is characterized by a wider variation of altitudinal gradient ranging from 450 to above 4000 m above sea level (Fig. 1). Because it is well known that the complex terrain regulates the
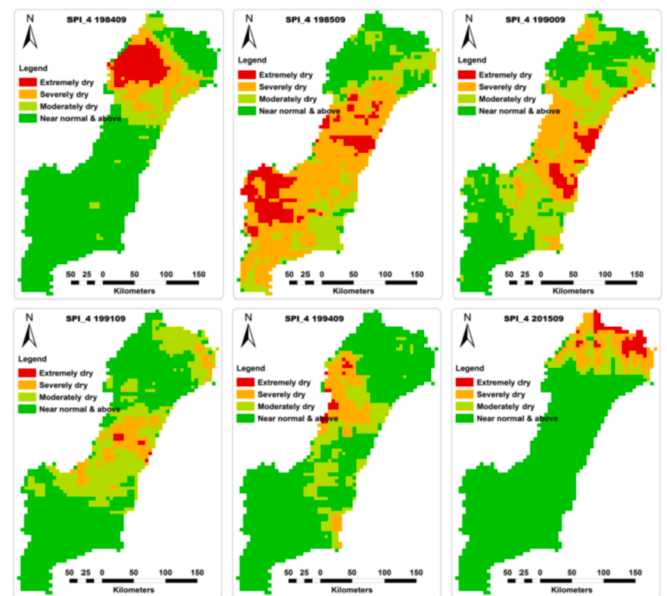

Fig. 11. Spatial distribution and intensities of historical drought events at 4-month time scale SPI in the *Kiremt* (June–September) season (only most severe drought events are shown).

Ethiopian climate by creating numerous microclimates having different amounts of rainfall (Viste, 2012; Jury, 2010; Dinku et al., 2007; Degefu and Glantz, 1987).

Another evident factor for the rainfall variability and subsequent droughts observed in the basin could be associated with climate variability exhibited as a reduction in the length or duration of the growing seasons. For instance, in the northern part of the present study area, Kassie, Rötter (Kassie et al., 2013) have reported a great inter-annual variability in the length of both rainy seasons (ranging from 76 to 239 days), with longer dry spells in the *Belg* season. In turn, this may be partially caused by late onset and early termination of rains which makes difficult for rain-fed producers to certainly decide the appropriate planting time (Kassie et al., 2013). Such variable duration in the length of the growing seasons and unpredictable start and termination of rainfall inevitably affects the amount and spatial distribution of rainfall, subsequently leading to drought incidences as already observed in this study. Similar declining trends in the length of the growing seasons was also reported in other parts of the country (World-Bank, 2006; Araya and Stroosnijder, 2011; Segele and Lamb, 2005). For instance, World-Bank (2006) specifically reported that the late start of the *Kiremt* rain in 1997 resulted in average yield reduction of cereals by 10% nationally in Ethiopia.

In the meantime, statistically significant rising trends of air temperature were observed in the basin at majority of the weather stations mainly during the growing seasons. Such a significant warming trend during the growing seasons could further intensify drought conditions as it obviously raises the rate of evapotranspiration.

In turn, the root cause of the inter-annual rainfall variability and frequent drought incidences observed in the study area could be further associated with global sea surface temperature and pressure anomalies occurred in relevant oceans. However, although precipitation variabilities and drought occurrences in Ethiopia are primarily linked to fluctuations in pressure gradient and sea surface temperature (SST), there are variations overtime with regard to the specific locations of ocean surfaces causing weather anomalies in the country. For example, in earlier times, the decline in summer or *Kiremt* precipitation which caused for instance the 1984 devastating drought, was very strongly correlated to variability in sea level pressure (SLP) gradient between the Sudan and the southern coast of the Mediterranean sea (Williams et al., 2012). However, the relationships between regional precipitation and
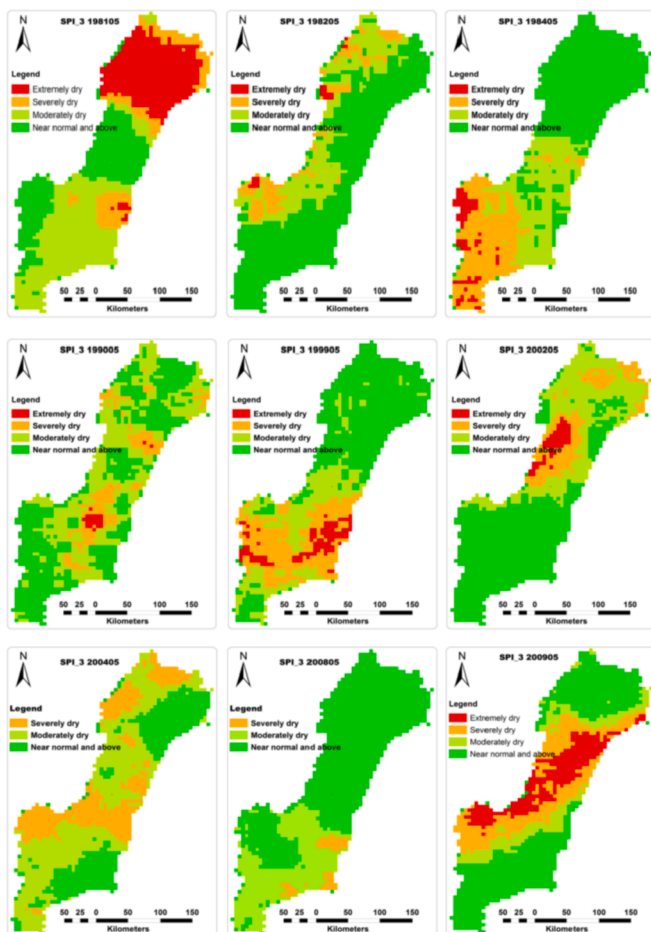

Fig. 10. Spatial distribution and intensities of historical drought events at 3-month time scale SPI in the *Belg* (March–May) season (only most severe drought events are shown here).

the influence of these SLP indices were weakened in recent years, generally in the horn of Africa. This trend was exhibited for instance, during the 1990–2009, when mean June–September rainfall totals in the Horn of Africa continued to decline while the SLP indices were more favorable for precipitation conditions (Williams et al., 2012). On the other hand, air masses carrying moisture from the Indian Ocean, Atlantic Ocean, as well as the Red Sea continued to be important components of the summer (*Kiremt*) rain in Ethiopia (Viste, 2012).

Earlier evaluations of trends in atmospheric circulation and moisture transports in the horn of Africa in general show that warming in the southern tropical Indian Ocean (STIO) accounts for a substantial portion of the recent rainfall declines in the region (Funk et al, 2008, 2014a; Williams et al., 2012; Alory et al., 2007; Cai et al., 2007; Verdin et al., 2005; Barnett et al., 2001). Because, although anthropogenic warming has affected all oceans (Barnett et al., 2001), the warming has been larger in the Indian Ocean (Cai et al., 2007), where an increase in SST of 0.5–1.0 °C was observed between 1960 and 1999 (Alory et al., 2007). As a result, further warming occurred in the previously warm STIO during the past half century has led to a large increase in STIO evaporation and remarkable increase in STIO precipitation, causing decreased easterly moisture flow towards eastern Africa (Williams et al., 2012; Verdin et al., 2005). Similarly, the emergence of more warm areas in the equatorial Pacific ocean was also tied to an increase in local precipitation over that ocean and reduced rainfall over Eastern Africa, including Ethiopia (Funk et al., 2014a; Verdin et al., 2005).

Specifically, recent studies have investigated the teleconnection between fluctuations in SSTs and the Ethiopian rainfall both in the *Belg* and *Kiremt* seasons (Degefu et al., 2017; Fekadu, 2015). Accordingly, the *Kiremt* rain in Ethiopia was negatively associated with SST fluctuations over the equatorial Pacific, the Indian Ocean Dipole (IOD), and central Indian Ocean index (CIndO). The relationship with the IOD and CIndO was however limited to the western part of the country (Degefu et al., 2017) which is outside of the present study area. As a result, the rainfall variability and frequent drought episodes observed in the study area could be primarily linked to SST fluctuations in the equatorial Pacific Ocean. Because, during El Niño episodes (warm phase ENSO) in the equatorial Pacific Ocean, the *Kiremt* (June–September) rainfall in the country in general declines to below average, causing droughts during strong El Niño years (Degefu et al., 2017; Fekadu, 2015). In contrast, La Niña events (cold phase ENSO) favors further temporal expansion of the rainy season beyond the normal *Kiremt* duration of a given area (Fekadu, 2015). Similarly, it was reported that a clear link was established between ENSO and the *Belg* rain in Ethiopia. During the La Niña state, the main beneficiaries of *Belg* rain in the country experience shortage of rainfall while during El Niño situation, most of the *Belg* rainfall recipients receive higher amount of rainfall (Fekadu, 2015). Thus, the frequent drought incidence in the study area during the *Belg* and *Kiremt* seasons could be primarily linked to the La Niña and El Niño situations, respectively.

Furthermore, due to such fluctuations in SSTs, further declines in rainfall amount are likely to occur generally in the country (Funk et al., 2008). For instance, the climate change projections made by IPCC (IPCC, 2014) forecasted a rise in CO_2 and associated greenhouse gases could lead to a rise in global surface temperatures of up to 5.8 °C in 2100 compared to the preindustrial baseline. Such expected global warming could have direct impacts on the amount and spatial distribution of rainfall. The significant warming observed in the study area could also be one of the manifestations of the borderless global warming. Therefore, the impacts of the projected further climate change, as already observed in the past, could have more pronounced consequences in countries like Ethiopia, particularly the study area due to the strong dependence on rain-fed agriculture. This in turn, necessitates well preparedness for designing of drought mitigation and early warning systems.

5. Conclusions

The study focuses on evaluation of long term rainfall and temperature variabilities, trends, and subsequent meteorological drought events in order to understand and characterize climate variability in the Ethiopian rift valley lakes basin. To realize this objective, the analysis was carried out across the major agroecological zones in the basin. Accordingly, coefficient of variation and standardized rainfall anomaly were used to evaluate rainfall variability while Mann-Kendall test was employed to understand the trends of rainfall and temperature overtime. Similarly, the standardized precipitation index (SPI) (McKee et al., 1993) was used as a measure of drought assessment. Instead of the conventionally used sparse and unevenly distributed rain gauge data, a blended satellite-gauge rainfall grid was used to compute pixel-based SPI, which greatly helps to understand the spatial distribution and assess the environmental and socioeconomic impacts of drought events. Thus, the SPI was computed for 37 years (1981–2017) for the bimodal rainy seasons (*Belg* and *Kiremt*) that determine rain-fed agricultural production in the study area.

The result shows a strong spatial correlation between the high interannual variability of rainfall and the spatiotemporal distributions of meteorological droughts. All agroecological zones in the basin were stricken at least partially by the historical drought events but with varying frequency and intensity. Generally, more frequent droughts were observed in the basin compared to the nationally documented historical drought events, which implies higher vulnerability of the basin to climate variability. As a result, over the 1981–2017, at least a moderate drought intensity was occurred in various parts of the study area, on average every 1.68 and 1.76 years in the *Belg* and *Kiremt* seasons, respectively. Besides, the study area was often stricken by long lasting droughts persisting both in the spring and summer seasons, which could substantially affect the rain-fed agriculture in the basin. For instance, such a situation was observed in 1981, 1983, 1984, 1985, 1988, 1990, 1991, 1995, 2001, 2002, and 2003.

Temporally, the frequency of drought incidence in both rainy seasons was higher in the 1980s, compared to the 1990s and 2000s, but it was not statistically significant at 0.05 significance level. In addition, the spatial patterns of drought events to some extent has followed seasonal patterns of rainfall distributions. For example, the frequency of drought incidence in the southern part of the basin was higher during the *Belg* (main rainy season in the southern part). Whereas in the central and northern parts of the basin, drought frequency was almost similar in both seasons.

On the other hand, due to microclimate differences, local variations across AEZs were observed with regard to the frequency and spatial distribution of drought events. As a result, the *Kolla* AEZ, characterized by higher coefficient of rainfall variation, was stricken more frequently in both rainy seasons than the *Dega* and *Weyna Dega* AEZs, relatively characterized by lower CV. This could be linked to the prevalence of orographic rainfall where the highland AEZs receive relatively higher amount of rainfall than the adjacent lowlands. Still, a great variation in the spatial distribution and intensity of drought events was found even within the lowland agroecology. Therefore, more localized or watershed-based planning of drought adaptation strategies could be more appropriate to alleviate drought impacts in the basin.

Furthermore, the study area has undergone statistically significant rises in monthly air temperatures over several months. Such a rising temperature trend coupled with the impacts of unavoidable global climate change (IPCC, 2014; Altieri et al., 2015) could aggravate future drought conditions in the basin by accelerating evapotranspiration rates, having direct implications on soil moisture and crop growth. Thus, effective implementations of afforestation including urban greenery programs are potentially important to modulate the local microclimates. Generally, integrated efforts focusing on the design of diverse and relevant drought adaptation strategies could help to best address the potential impacts of climate extremes likely to persist in the basin.

Diversification of drought adaptation strategies could be more effective in coping up drought impacts as the study area consists of various AEZs and livelihoods. To this end, the findings of this study, which shows the spatial variabilities of annual and seasonal rainfall and the spatiotemporal distributions of associated meteorological droughts, could greatly enhance the awareness of concerned decision makers to devise relevant strategies for mitigation and adaption of future drought episodes in the basin.

Declaration of competing interest

The authors declare that they do not have any conflict of interest.

Acknowledgements

References

Agnew, C.T., Chappell, A., 1999. Drought in the Sahel. Geojournal 48, 299–311, 1999.

Agricultural Transformation Agency, 2014. Transforming Agriculture in Ethiopia: Agricultural Transformation Agency. Annual report.

Alory, G., Wijffels, S., Meyers, G., 2007. Observed temperature trends in the Indian Ocean over 1960–1999 and associated mechanisms. Geophys. Res. Lett. 34, L02606. https://doi.org/10.1029/2006GL028044.

Altieri, M.A., 1995. Agroecology: the Science of Sustainable Agriculture. Westview Process, Boulder.

Altieri, M.A., et al., 2015. Agroecology and the design of climate change-resilient farming systems: review article. Agron. Sustain. Dev. https://doi.org/10.1007/s13593-015-0285-2. Springer.

Araya, A., Stroosnijder, L., 2011. Assessing drought risk and irrigation need in northern Ethiopia. Agric. For. Meteorol. 151, 425–436.

Asfaw, A., et al., 2018. Variability and time series trend analysis of rainfall and temperature in northcentral Ethiopia: a case study in Woleka sub-basin. Weather and Climate Extremes 19, 29–41, 2018.

Ayehu, G.T., et al., 2018. Validation of new satellite rainfall products over the upper blue nile basin, Ethiopia. Atmos. Meas. Tech. 11, 1921–1936. https://doi.org/10.5194/amt-11-1921-2018, 2018.

Bannayan, M., et al., 2010. Association between climate indices, aridity index and rain-fed crop yield in northeast of Iran. Field Crop. Res. 118, 105–114. https://doi.org/10.1016/j.fcr.2010.04.011.

Barnett, T.P., Pierce, D.W., Schnur, R., 2001. Detection of anthropogenic climate change in the World's oceans. Science 292, 270–274. https://doi.org/10.1126/science.1058304.

Bayissa, Y., et al., 2017. Evaluation of satellite-based rainfall estimates and application to monitor meteorological drought for the Upper Blue Nile Basin, Ethiopia. Remote Sens. 9 (7), 669.

Boko, M., et al., 2007. In: Parry, M.L., Canziani, O.F., Palutikof, J.P., van der Linden, P.J., Hanson, C.E. (Eds.), Climate Change 2007: Impacts, Adaptation and Vulnerability. Contribution of Working Group II to the Fourth Assessment Report of the Intergovernmental Panel on Climate Change. Cambridge University Press, Cambridge UK, pp. 433–467.

Cai, W., et al., 2007. Anthropogenic aerosol forcing and the structure of temperature trends in the southern Indian Ocean. Geophys. Res. Lett. 34, L14611. https://doi.org/10.1029/2007GL030380.

Chattopadhyay, S., Edwards, D.R., 2016. Long-term trend analysis of precipitation and air temperature for Kentucky, United States. Climate 4, 10. https://doi.org/10.3390/cli4010010.

Degefu, M.A., Bewket, W., 2014. Trends and spatial patterns of drought incidence in the Omo-Ghibe River Basin, Ethiopia. Geogr. Ann. Ser. A Phys. Geogr. 97, 395–414. https://doi.org/10.1111/geoa.12080.

Degefu, W., 1987. Some aspects of meteorological drought in Ethiopia. In: Glantz, M.H. (Ed.), Drought and Hunger in Africa: Denying Famine a Future. Press Syndicate of the University of Cambridge, Cambridge, pp. 223–236.

Degefu, M.A., Rowell, D.P., Bewket, W., 2017. Teleconnections between Ethiopian rainfall variability and global SSTs: observations and methods for model evaluation. Meteorol. Atmos. Phys. 129, 173–186. https://doi.org/10.1007/s00703-016-0466-9, 2017.

Dembélé, M., Zwart, S.J., 2016. Evaluation and comparison of satellite-based rainfall products in Burkina Faso, West Africa. Int. J. Remote Sens. 37 (17), 3995–4014. https://doi.org/10.1080/01431161.2016.1207258.

Dinku, T., et al., 2007. Validation of satellite rainfall products over East Africa's complex topography. Int. J. Remote Sens. 28, 1503–1526.

Dinku, T., et al., 2008. Validation of high-resolution satellite rainfall products over complex terrain in Africa. Int. J. Remote Sens. 29, 4097–4110.

Dinku, T., et al., 2013. Combined use of satellite estimates and rain gauge observations to generate high-quality historical rainfall time series over Ethiopia. Int. J. Climatol. https://doi.org/10.1002/joc.3855.

Dinku, T., et al., 2018. Validation of the CHIRPS Satellite Rainfall Estimates over Eastern Africa. Royal Meteorological Society. https://doi.org/10.1002/qj.3244.

Edossa, D.C., Babel, M.S., Gupta, A.D., 2010. Drought analysis in the Awash river basin. Ethiopia Water Resource Management 24, 1441–1460. https://doi.org/10.1007/s11269-009-9508-0.

Eerens, H., Haesen, D., 2016. Software for the Processing and Interpretation of Remotely Sensed Image Time Series (SPIRITS) User's Manual Version: 1.5.0. Vision on Technology (VITO). Institute for environment and sustainability. JRC European commission.

Fekadu, K., 2015. Ethiopian seasonal rainfall variability and prediction using canonical correlation analysis (CCA). Earth Sci. 4 (3), 112–119. https://doi.org/10.11648/j.earth.20150403.14.

Funk, C., et al., 2005. Recent drought tendencies in Ethiopia and equatorial-subtropical eastern Africa, 1. FEWS NET.

Funk, C., et al., 2008. Warming of the Indian Ocean threatens eastern and southern Africa, but could be mitigated by agricultural development. Physical Sciences, Sustainability Science. https://ntrs.nasa.gov/search.jsp?R=20080023358 2018-08-02T09:40:34+00:00Z.

Funk, C., et al., 2014. Predicting East African spring droughts using Pacific and Indian Ocean sea surface temperature indices. Hydrol. Earth Syst. Sci. Discuss. 11, 3111–3136. https://doi.org/10.5194/hessd-11-3111-2014. www.hydrol-earth-syst-sci-discuss.net/11/3111/2014/.

Funk, C.C., et al., 2014. A quasi-global precipitation time series for drought monitoring. U.S. Geological Survey Data Series 832, 4. https://doi.org/10.3133/ds832.

Funk, C., et al., 2015. The climate hazards infrared precipitation with stations—a new environmental record for monitoring extremes. Scientific Data 2, 150066. https://doi.org/10.1038/sdata.2015.66. www.nature.com/scientificdata.

Gebrehiwot, T., van der Veena, A., Maathuis, B., 2011. Spatial and temporal assessment of drought in the Northern highlands of Ethiopia. Int. J. Appl. Earth Obs. Geoinf. 13, 309–321, 2011.

Gidey, E., et al., 2018. Predictions of Future Meteorological Drought Hazard (∼ 2070) under the Representative Concentration Path (RCP) 4.5 Climate Change Scenarios in Raya. Modeling Earth Systems and Environment. Springer. https://doi.org/10.1007/s40808-018-0453-x.

Gilbert, R.O., 1987. Statistical Methods for Environmental Pollution Monitoring. USA: Van Nostrand Reinhold Company, New York, ISBN 0-442-23050-8.

Guttman, N.B., 1998. Comparing the palmer drought index and the standardized precipitation index. J. Am. Water Resour. Assoc. 34 (1), 113–121.

Hadgu, G., et al., 2013. Trend and variability of rainfall in Tigray, Northern Ethiopia: analysis of meteorological data and farmers' perception. Acad. J. Agric. Res. 1 (6), 088–100. https://doi.org/10.15413/ajar.2013.0117 ISSN: 2315-7739.

Hayes, M.J., 2000. Revisiting the SPI: Clarifying the Process Drought Network News (1994-2001). Paper 18. http://digitalcommons.unl.edu/droughtnetnews/18.

Hurni, H., 1998. Agroecological Belts of Ethiopia Explanatory Notes on Three Maps at a Scale of 1:1,000,000. Soil Conservation Research Programme Ethiopia Research Report.

IPCC, 2014. Climate Change 2014 Mitigation of Climate Change Summary for Policymakers and Technical Summary. Intergovernmental panel on climate change.

Jury, M.R., 2010. Ethiopian decadal climate variability. Theor. Appl. Climatol. 101, 29–40. https://doi.org/10.1007/s00704-009-0200-3, 2010.

Kassie, B.T., et al., 2013. Climate variability and change in the Central Rift Valley of Ethiopia: challenges for rainfed crop production. J. Agric. Sci. 152, 58–74. https://doi.org/10.1017/S0021859612000986. © Cambridge University Press, 2013.

Kendall, M.G., 1975. Rank Correlation Methods, fourth ed. Charles Griffin, London.

Kidd, C., Huffman, G., 2011. Review - global precipitation measurement. Meteorol. Appl. 18, 334–353. https://doi.org/10.1002/met.284.

Kidd, C., Levizzani, V., 2011. Status of satellite precipitation retrievals. Hydrol. Earth Syst. Sci. https://doi.org/10.5194/hess-15-1109-2011.

Lopez, M.G., et al., 2015. Location and density of rain gauges for the estimation of spatial varying precipitation. Geogr. Ann. Ser. A Phys. Geogr. 97 https://doi.org/10.1111/geoa.12094, 2015.

Luana, S., Hou, X., Wang, Y., 2015. Assessing the accuracy of srtm dem and aster gdem datasets for the coastal zone of shandong province, Eastern China. Polish maritime research Special Issue 22 (86), 15–20. https://doi.org/10.1515/pomr-2015-0026, 2015 S1, 2015.

Mann, H.B., 1945. Nonparametric tests against trend. Econometrica. Journal of the Econometric Society 13, 245–259.

McKee, T.M., Doesken, N.J., Kleist, J., 1993. The relationship of drought frequency and duration to time scales. Eighth Conference on Applied Climatology (January), 17–22, 1993, Anaheim, California.

Mishra, A.K., 2013. Effect of rain gauge density over the accuracy of rainfall: a case study over Bangalore, India. SpringerPlus 2, 311, 2013. http://www.springerplus.com/content/2/1/311.

Mohammed, Y., et al., 2017. Meteorological drought assessment in north east highlands of Ethiopia. International Journal of Climate Change Strategies and Management. https://doi.org/10.1108/IJCCSM-12-2016-0179.

Molla, M.B., Ikporukpo, C.O., Olatubara, C.O., 2018. The spatio-temporal pattern of urban green spaces in southern Ethiopia. Am. J. Geogr. Inf. Syst. 7 (1), 1–14. https://doi.org/10.5923/j.ajgis.20180701.01, 2018.

MoWE, 2014. River basins of Ethiopia: basin description thematic maps. Ethiopian Ministry of Water Resources and Energy. September, 2017. http://www.mowr.gov. et.

NASA Overview of SRTM, ASTER DEM Data, 2017. NASA's Applied Remote Sensing Training Program.

Segele, Z.T., Lamb, P.J., 2005. Characterization and variability of Kiremt rainy season over Ethiopia. Meteorol. Atmos. Phys. 89, 153–180.

Sen, P.K., 1968. Estimates of regression coefficients based on Kendall's tau. J. Am. Stat. Assoc. 63, 1379–1389.

Tesfamariam, B.G., Melgani, F., Gessesse, B., 2019. Rainfall retrieval and drought monitoring skill of satellite rainfall estimates in the Ethiopian Rift Valley Lakes Basin. J. Appl. Remote Sens. 13 (1) https://doi.org/10.1117/1.JRS.13.014522.

Thornton, P.K., et al., 1934. Agriculture and food systems in sub-Saharan Africa in a 4 degrees C+ world. Philos. Trans. R. Soc. A Math. Phys. Eng. Sci. 369, 117–136. ISSN 1364-503X, 2011.

Toté, C., et al., 2015. Evaluation of satellite rainfall estimates for drought and flood monitoring in Mozambique. Remote Sens. 7, 1758–1776. https://doi.org/10.3390/ rs70201758, 2015.

Trejo, F.J.P., et al., 2016. Intercomparison of improved satellite rainfall estimation with CHIRPS gridded product and rain gauge data over Venezuela. Atmósfera 29 (4), 323–342. https://doi.org/10.20937/ATM.2016.29.04.04, 2016.

USAID, A., 2012. Climate trend Analysis of Ethiopia: famine early warning systems network—informing climate change adaptation series. FEWS NET, USGS, Science for a changing world 2012–3053. Fact Sheet.

Verdin, J., et al., 2005. Climate science and famine early warning. Phil. Trans. R. Soc. B 360, 2155–2168. https://doi.org/10.1098/rstb.2005.1754.

Viste, E., 2012. Moisture Transport and Precipitation in Ethiopia,Dissertation for the Degree Philosophiae Doctor. PhD) University of Bergen, Norway.

Viste, E., Korecha, D., Sorteberg, A., 2013. Recent drought and precipitation tendencies in Ethiopia. Theor. Appl. Climatol. 112, 535–551. https://doi.org/10.1007/s00704-012-0746-3.

Wilhite, D.A., 1993. Understanding the Phenomenon of Drought. Drought Mitigation Center Faculty Publications, p. 50. http://digitalcommons.unl.edu/droughtfacpub/ 50.

Williams, A.P., et al., 2012. Recent summer precipitation trends in the Greater Horn of Africa and the emerging role of Indian Ocean sea surface temperature. Clim. Dyn. 39, 2307–2328. https://doi.org/10.1007/s00382-011-1222-y, 2011.

WMO, 2012. Standardized Precipitation Index User Guide. World Meteorological Organization, WMO-No. 1090, Geneva.

World-Bank, 2006. Managing Water Resources to Maximise Sustainable Growth: A Country Water Resources Assistance Strategy for Ethiopia. World Bank, Washington, DC.

Zargar, A., et al., 2011. A review of drought indices. Environ. Rev. 19, 333–349.